Naval Research Laboratory

Washington, DC 20375-5000

NRL Memorandum Report 6338

Final Focusing of Intense Ion Beams with Radially Nonuniform Current Density Z-Discharges

J. J. WATROUS

National Research Council
Naval Research Laboratory
Research Associate

P. F. OTTINGER

Plasma Technology Branch
Plasma Physics Division

October 26, 1988

SECURITY CLASSIFICATION OF THIS PAGE

REPORT DOCUMENTATION PAGE

Form Approved
OMB No 0704-0188

1a REPORT SECURITY CLASSIFICATION UNCLASSIFIED	1b RESTRICTIVE MARKINGS
2a SECURITY CLASSIFICATION AUTHORITY	3 DISTRIBUTION / AVAILABILITY OF REPORT Approved for public release; distribution unlimited.
2b DECLASSIFICATION / DOWNGRADING SCHEDULE	
4 PERFORMING ORGANIZATION REPORT NUMBER(S) NRL Memorandum Report 6338	5 MONITORING ORGANIZATION REPORT NUMBER(S)
6a NAME OF PERFORMING ORGANIZATION Naval Research Laboratory 6b OFFICE SYMBOL (If applicable) Code 4770	7a NAME OF MONITORING ORGANIZATION
6c ADDRESS (City, State, and ZIP Code) Washington, DC 20375-5000	7b ADDRESS (City, State, and ZIP Code)
8a NAME OF FUNDING / SPONSORING ORGANIZATION DOE 8b OFFICE SYMBOL (If applicable)	9 PROCUREMENT INSTRUMENT IDENTIFICATION NUMBER
8c ADDRESS (City, State, and ZIP Code) Washington, DC 20545	10 SOURCE OF FUNDING NUMBERS PROGRAM ELEMENT NO: DE AI 08-79 PROJECT NO: DP40092 TASK NO: WORK UNIT ACCESSION NO: DN680-382

11 TITLE (Include Security Classification) Final Focusing of Intense Ion Beams with Radially Nonuniform Current Density Z-Discharges

12 PERSONAL AUTHOR(S)
Watrous,* J. and Ottinger, P.F.

13a TYPE OF REPORT	13b TIME COVERED	14 DATE OF REPORT (Year, Month, Day)	15 PAGE COUNT
Interim	FROM _____ TO _____	1988 October 26	43

16 SUPPLEMENTARY NOTATION
Identical manuscript submitted for publication in The Physics of Fluids.
*National Research Council/Naval Research Laboratory Associate

17 COSATI CODES			18 SUBJECT TERMS (Continue on reverse if necessary and identify by block number)
FIELD	GROUP	SUB-GROUP	Ion beams, Z-discharges, Focusing

19 ABSTRACT (Continue on reverse if necessary and identify by block number)

The spotsize and focal length of a one-eighth betatron wavelength final focusing cell with a nonuniform current density distribution are predicted. The predictions are based on a Lie Transform solution to the equations of motion of an ion in an azimuthal magentic field that models various distributions of the discharge current density. The solution to the nonlinear equations of motion is coupled to a simple phase space concept that yields both the minimum spotsize and focal length of the final focusing cell. The analysis indicates that a final focusing cell with a current density distribution that is strongly concentrated at the channel edge focuses the beam much less efficiently than a channel with a uniform current density distribution. Quantitatively, by employing a simple model azimuthal magnetic field distribution of the form $B_\theta(r) \propto r^N$, the analysis provides an approximate relation between the focused beam radius (r_{foc}), the unfocused beam radius (r_c), and the ratio of discharge current in the focusing cell (I_f) to that in the transport channel (I_c): $r_{foc} \sim r_c\,(I_c/I_f)^{1/2N}$.

20 DISTRIBUTION / AVAILABILITY OF ABSTRACT	21 ABSTRACT SECURITY CLASSIFICATION
☒ UNCLASSIFIED/UNLIMITED ☐ SAME AS RPT ☐ DTIC USERS	UNCLASSIFIED
22a NAME OF RESPONSIBLE INDIVIDUAL P.F. Ottinger	22b TELEPHONE (Include Area Code) (202) 767-3066 22c OFFICE SYMBOL Code 4770

DD Form 1473, JUN 86 *Previous editions are obsolete.* SECURITY CLASSIFICATION OF THIS PAGE

S/N 0102-LF-014-6603

1/2 N+1

CONTENTS

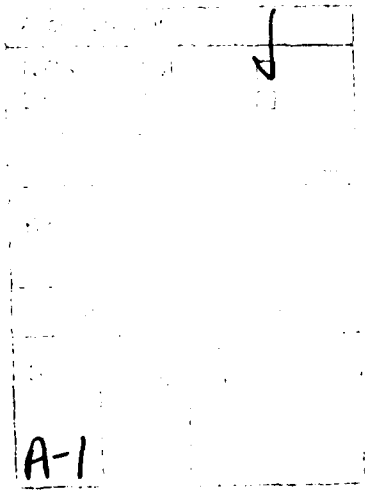

FINAL FOCUSING OF INTENSE ION BEAMS WITH RADIALLY NONUNIFORM CURRENT DENSITY Z-DISCHARGES

I. INTRODUCTION

The Advanced Pulse Experiment (APEX Project) at Sandia National Laboratories will test several concepts crucial to the success of light ion beam inertial confinement fusion[1]. As currently envisioned, the experiment will employ z-discharge channel transport of intense ion beams from the accelerator to the target. Previous analyses of ion beam transport in z-discharge plasma channels indicate that in order to avoid many of the effects that could degrade the beam quality, the beam should be transported in a large radius (2 - 3 cm) channel[2]. Because of the mismatch between the target radius (~0.5 cm) and the beam radius after transport in a large radius channel, some method of final focusing must be used to reduce the ion beam radius.

A proposed method for final focusing is to have the ion beam pass from the long (3-10 m), low current (~50 kA) z-discharge transport channel directly into a short (~5 cm), high current (~500 kA) z-discharge[3]. The sudden increase in magnetic field strength causes the ion beam to pinch inward. By fixing the length of the focusing cell to be one eighth of a beam ion betatron wavelength, this pinching effect allows the ion beam to come to a focus at a short distance (~5 cm) downstream from the focusing cell exit. This method of focusing is referred to as one-eighth betatron wavelength focusing, and has been referred to in the past as final focusing.

A previous analysis of the one-eighth betatron wavelength focusing method predicted the spotsize, the focal length, and the radial beam number density profile at the focal plane[3,4]. The spotsize, or equivalently, the radial beam compression ratio was predicted to be

Manuscript approved August 31, 1988.

$$\left(r_{foc}/r_c\right)^2 = 2 / (1 + R) \qquad (1)$$

where r_{foc} is the radius of the beam at the focal plane, r_c is the radius of the transport channel and focusing cell, and R is the ratio of the focusing cell discharge current, I_f, to the transport channel discharge current, I_c. The focal length, that is, the distance between the exit of the focusing cell and the focal plane, was predicted to be

$$z_{foc} = \left(\frac{R - 1}{R + 1}\right) \lambda_\beta / 2\pi \qquad (2)$$

where λ_β is the betatron wavelength of a beam ion in the focusing cell. This analysis was based on the assumption that the discharge current density in the focusing cell was uniformly distributed within the radius of the discharge.

A new analysis has been performed to determine how the spotsize and focal length of the focusing cell change when the discharge current density distribution is not uniform. For this analysis, a model azimuthal magnetic field distribution of the form

$$B_\theta(r) = \frac{2I_f}{cr_c} \left(\frac{r}{r_c}\right)^N \qquad (3)$$

is used, where I_f is the discharge current of the final focusing cell and c is the speed of ligh' The case with N = 1 corresponds to a uniform discharge current density, and will be referred to as the ideal distribution. The reason for studying different magnetic field profiles is that it may not always be possible to obtain the ideal magnetic field distribution in an experiment. For example, in beam transport experiments at the Naval Research Laboratory, B_θ profiles in the transport channel approximately of the form $(r/r_c)^2$ have been observed[5]. Theoretical models of the time-dependent diffusion of the magnetic field into a z-discharge plasma also indicate that at early times in the development of the discharge, the azimuthal magnetic field has a radial profile that may be approximately described Eq. (3), where larger values of N correspond to earlier times in the development of the discharge. To interpret the results of beam focusing experiments, it will be valuable to have a prediction of the spotsize and focal length of nonideal focusing cells.

In Section II of this paper, the general method used for predicting the spotsize and focal length of a focusing cel' is described. In Section III, the equations of motion for an ion in an r^N magnetic field distribution are solved using a Lie transform technique, and are applied to the method described in Section II to give the predictions of spotsize and focal length. Finally, in Section IV these predictions are compared with the results of numerical simulations of ion beam focusing.

II. The Theoretical Basis for the Prediction of the Spotsize and the Focal Length

The spotsize and the focal length that characterize the focusing properties of the final focusing cell can be predicted on the basis of the manner in which that focusing cell alters the radial phase space distribution of the ion beam as it passes through the cell. In this Section the relation between the ion beam radial phase space distribution, the spotsize and the focal length will be developed. This discussion will be based on the assumptions that the beam is composed of monoenergetic ions with zero angular momentum, that the beam propagates in a fully current and charge neutralized mode, and that the beam is produced by a time-independent source.

Under the assumptions noted above, the propagation of the beam can be fully characterized by a description of its radial phase space distribution at any given location along the propagation axis, and this description can be made on the basis of the single particle motions of a beam ion in the magnetic field structure of the transport channel and of the final focusing cell. It will be assumed that in the transport channel, the distribution of the magnetic field is given by the ideal distribution, i.e. $B_\theta(r) = (2I_c/cr_c)\times(r/r_c)$. In this azimuthal magnetic field structure, the trajectory of a beam ion is a periodic, approximately sinusoidal trajectory known as a betatron orbit. The betatron orbit can be understood as a grad-B drift. A beam ion injected parallel to the channel axis at the channel radius feels the full strength of the magnetic field and begins to execute a gyromotion that moves the ion both down the length of the channel and in toward the channel axis. As the ion moves inward, it feels a weaker magnetic field so that, at that instant, the ion is on a gyro-orbit with a radius of curvature somewhat larger than what it was at the channel entrance. When

the ion reaches the channel axis, the magnetic field strength is zero so that the radius of curvature of the gyro-orbit is infinite. The momentum of the ion carries it across the channel axis into a region of increasing magnetic field strength, so that the instantaneous radius of curvature of the trajectory decreases as a function of time. The ion reaches the side of the channel opposite to that from which it started and begins to fall back toward the axis. The axial distance required for an ion to complete one cycle of this periodic motion is called the betatron wavelength, and is a function of an ion's maximum radial excursion, or turning point. The larger the turning point of an ion is, the shorter its the betatron wavelength is. The radial phase space distribution of the propagating ion beam is approximately periodic in the propagation distance due to the periodic nature of the single particle trajectories. Thus, at intervals of the betatron wavelength, the initial radial phase space distribution reappears. However, due to the dependence of the betatron wavelength on the turning point, the periodic reappearences of the initial distribution are accompanied by a gradual deformation of that distribution. Ions with larger turning points lag in phase slightly behind those with smaller turning points. The eventual outcome of this phase mixing is that the radial phase space distribution becomes homogenized over the phase angle in the radial phase space plane. It will be assumed in this work that the transport channel is sufficiently long so that the beam becomes completely phase mixed before it reaches the final focusing cell. The radial phase space distribution of the fully phase mixed ion beam fills an elliptical region of the radial phase space plane defined by

$$r^2 + \left(\frac{1}{kv_b}\right)^2 v_r^2 \leq r_c^2 \ , \qquad (4)$$

where v_b is the speed of a beam ion, r_c is the transport channel radius, and k is the betatron wavenumber defined by

$$k = 2\pi/\lambda_\beta = \left(\frac{2ZeI_c}{Am_p c^2 v_b r_c^2}\right)^{1/2}, \qquad (5)$$

where m_p is the proton mass, e is the proton charge, and A and Z are the mass and atomic numbers of the beam ion, respectively. The distribution of ions inside this elliptical region is determined by the form of the initial radial phase space distribution, but this is not a matter of importance in this analysis. The item of main importance is Eq. (4), which defines the outer boundary of the phase mixed ion beam distribution in radial phase space.

When the ion beam reaches the final focusing cell, the sudden increase in the magnetic field strength and the sudden change in the magnetic field distribution cause the radial phase space distribution of the beam to begin to undergo a deformation. The exact nature of this deformation is the subject of Section III. For this discussion, it is not necessary to know these details other than that the deformation represents a continuous change in the originally elliptical boundary of the ion beam radial phase space distribution characterized by a skewing of the distribution toward negative radial velocities. At the exit of the final focusing cell, the ion beam radial phase space distribution has been deformed to some new shape that depends on the length of the cell, the final focusing cell discharge current, and the distribution of the magnetic field in the cell. After passing through the focusing cell, the beam propagates

ballistically for some distance before coming to the focal plane. Between the focusing cell exit and the focal plane, the ion beam radial phase space distribution continues to deform as individual ions follow straight line paths defined by constant values of the radial velocity. The ions that at the focusing cell exit had radial velocities equal to zero hold a special place in this process. All other ions either move away from the axis or move toward the axis, pass through it, then continue to move away from the axis. The ions that occupied the line $v_r = 0$ at the focusing cell exit move along lines of constant radius, and because of that, they define the smallest radius to which the ion beam can be focused. Thus, as illustrated in Figure 1, the minimum spotsize that a focusing cell can produce is defined by the intersection of the line $v_r = 0$ with the outer boundary of the ion beam radial phase space distribution.

Once the minimum spotsize is known, the next item of interest is how far downstream from the focusing cell exit the minimum spotsize is actually achieved. This distance, the focal length, can be obtained by following the deformation of the ion beam radial phase space distribution as the ion beam propagates ballistically. As the ions propagate ballistically, they move along lines of constant v_r so that ions on the line $v_r = 0$ remain stationary in the radial phase space plane. As illustrated in Figure 2, the minimum spotsize is achieved when all ions with negative v_r have moved inside the spotsize radius and before any ion with positive v_r has passed beyond this radius. When this occurs the tangent to the radial phase space boundary curve is perpendicular to the v_r axis at the point where the curve passes through the v_r axis. Thus, the focal length can be defined as that axial location at which the radial phase space boundary curve has an infinite slope at the point where it intersects the v_r axis.

As an illustration of these concepts, consider the focusing of an ion beam with a one-eighth betatron wavelength focusing lens with the ideal magnetic field distribution. The boundary curve for the ion beam radial phase space distribution in the transport channel is given by Eq. (4) as discussed previously. In the focusing cell, the boundary curve is given by

$$r^2 + (y/K)^2 + (K^2/k^2 - 1)(r\sin(Kz) + (y/K)\cos(Kz))^2 = r_c^2 \qquad (6)$$

where K is the betatron wavenumber of a beam ion in the focusing cell (Eq. (5) with I_c replaced by I_f) and $y = v_r/v_b$. To find the spotsize, Eq. (6) is solved for $r = r_{foc}$ under the conditions $y = 0$, $z = (\pi/4)/K = \lambda_\beta/8$. The result is given by Eq. (1). To obtain the focal length, an equation describing the boundary curve in the ballistic drift region must be obtained. This is easily accomplished by substituting $r - zv_r/v_b$ for r in Eq. (6). Defining $\Delta = (I_f/I_c) - 1$, the boundary curve is given by

$$\left\{(2+\Delta)r^2 + \left[(2+\Delta)z^2 + (2+\Delta)/K^2 - 2\Delta z/K\right]y^2 + \left[2\Delta/K - 2(2+\Delta)z\right]yr\right\} = r_c^2 \qquad (7)$$

The next step is to operate through with $\partial/\partial r$ and solve for $\partial y/\partial r$. Evaluating the resulting expression at $y = 0$ gives

$$\left.\frac{\partial y}{\partial r}\right|_{y=0} = -\frac{(2 + \Delta)K}{[\Delta - (2 + \Delta)zK]} . \qquad (8)$$

This expression gives the slope of the curve that defines the outer boundary of the ion beam radial phase space distribution at the point where it intersects the v_r axis. The value of z at which this slope goes to $-\infty$ gives the focal length. By setting the denominator of the right hand side of Eq. (8) to zero, the required value of z is found to be $z = z_{foc}$ as given by Eq. (2).

To apply this method to a final focusing cell with a nonideal magnetic field distribution, it is necessary to have an expression for the curve that defines the outer boundary of the ion beam radial phase space distribution. This is the goal of Section III.

III. SOLUTION OF THE EQUATIONS OF MOTION

In order to apply the method described in Section II for predicting the spotsize and focal length, an equation describing the outer boundary of the ion beam's radial phase space distribution in the final focusing cell must be obtained. The curve that describes this boundary, which will be called the boundary curve, is the locus of points that define the radial phase space positions of ions at the outer edge of the beam radial phase space distribution. In the absence of collisions, as the beam travels through the transport channel, focusing cell, and on out into field free space, ions that were originally on the boundary curve remain on the boundary curve. Thus, the manner in which the boundary curve transforms in the focusing cell can be found by solving the equations of motion for ions in the focusing cell magnetic field. Eq. (4) gives an expression for that boundary curve for the ion beam in the transport channel after phase mixing, and Eq. (6) gives an expression for how that curve transforms in a focusing cell with the ideal magnetic field distribution. The goal of this Section is to find a result analogous to Eq. (6) that is applicable to a focusing cell with the model nonideal magnetic field distribution $B_\theta(r) = (2I_f/cr_c)\times(r/r_c)^N$. To illustrate the method used to obtain that result, a focusing cell with the ideal magnetic field distribution will be considered first.

The equations of motion for an ion with no angular momentum in the ideal magnetic field are

$$\frac{d^2r}{dt^2} = -\frac{q}{mc} B_o \frac{r}{r_c} v_z \tag{9a}$$

$$v_z = v_b - \frac{qB_o}{2mcr_c}(r_{tp}^2 - r^2) \tag{9b}$$

where B_o is the maximum magnetic field strength in the focusing cell, v_b is the magnitude of the ion's velocity, and r_{tp} is the ion's radial turning point. Eq. (9b) is an expression of the conservation of the canonical axial momentum. Inserting the expression for v_z given by Eq. (9b) into Eq. (9a) gives a single nonlinear equation for the ion's radial position as a function of time. The nonlinearity is a consequence of the variation of v_z with r given by Eq. (9b). This nonlinearity is the source of the dependence of the betatron wavelength on the turning point of an ion and is therefore important for analyzing the radial phase space dynamics of an ion beam propagating over distances of many betatron wavelengths, but for propagation over distances smaller than a betatron wavelength, such as in the final focusing cell, it is not important. For the present work this nonlinearity will be neglected. This gives a linearized radial equation of motion where v_z has been replaced by v_b:

$$\frac{d^2r}{dz^2} + \frac{1}{v_b}\left(\frac{qB_o}{mc}\right)\frac{r}{r_{ch}} = 0 \quad , \tag{10}$$

where, in addition, time t has been replaced by axial distance z via $t = z/v_b$. The solution to Eq. (10) is

$$r(z) = r_o\cos(Kz) + (y_o/K)\sin(Kz) \tag{11a}$$

$$y(z) = y_o\cos(Kz) - (r_o/r_{ch})\sin(Kz) \tag{11b}$$

where $r_o = r(0)$, $y_o = v_r(0)/v_b$, and K is the betatron wavenumber

of a beam ion in the final focusing cell. The boundary curve at the entrance of the focusing cell is, from Eq. (4),

$$r_o^2 + (y_o/k)^2 = r_{ch}^2 \qquad (12)$$

Eqs. (11a) and (11b) can be inverted to give r_o and y_o in terms of r(z) and y(z). These expressions are then substituted into Eq. (12) to give the expression for the boundary curve in the final focusing cell (Eq. (6)).

The mathematical result expressed by Eq. (6) indicates that in the ideal magnetic field distribution, the boundary curve undergoes a rigid rotation as the beam moves through the final focusing cell. This result has a simple physical interpretation. The change in the radial velocity of an ion as it enters the final focusing cell is proportional to the magnetic field strength at the radial position of the ion. Since in the ideal magnetic field distribution, the magnetic field strength is proportional to the radius, the change in an ion's radial velocity is also proportional to its radial position. Thus, over a short time interval Δt, the change in the radial velocity of an ion is $\Delta v_r \sim -r\Delta t$. This, coupled with the fact that the accompanying change in the radial position of the ion is proportional to the ion's radial velocity, i.e. $\Delta r \sim v_r \Delta t$, leads to the rigid rotation that characterizes the deformation of the boundary curve in the ideal magnetic field distribution. This line of thought is useful for anticipating the results that should be obtained from the analysis of the nonideal magnetic field distribution. In the nonideal magnetic field, the change in the radial velocity of an ion is still proportional to the magnetic field strength at the radial position of the ion, but

now the magnetic field strength is not simply proportional to the radial position. Thus, over a short time interval the change in an ion's radial velocity is $\Delta v_r \sim -(r/r_c)^N \Delta t$. For an ion at small radius, the factor $(r/r_c)^N$ can be very small for $N > 1$ so that the change in the radial velocity of the ion will be small. However, an ion located at a radius close to the channel radius will be subject to nearly the full magnetic field strength, so that ion will experience a large change in radial velocity. The change in the radial position of an ion during this small time interval is still given by $\Delta r \sim v_r \Delta t$. Thus, while the horizontal deflection of an ion in the radial phase space plane is the same as it was in the ideal cell, the vertical deflection during this small time interval will be slight at small radii and large at larger radii. The result should be a sheared rotation, with the rotation angle being a rapidly increasing function of the initial radius.

From the discussion above, the procedure for obtaining the boundary curve is (1) to solve the equations of motion for an ion in the focusing cell, (2) to invert the solution to give the initial conditions in terms of the downstream solution, and (3) to substitute the result of the second step into Eq. (12). For the ideal magnetic field distribution, this procedure offered little analytic difficulty because of the very simple form of the radial equation of motion (Eq. 10). For the nonideal r^N magnetic field distribution however, the radial equation of motion is not so easily solved - it is an equation of the form $x'' + x^N = 0$. Fortunately there is a method for generating a series solution to this equation that suits the requirements of this analysis. That method will be illustrated first for the case of the ideal magnetic field distribution, then will be applied to the nonideal field.

Eq. (10) can be written as a pair of first order differential equations:

$$\frac{dx}{ds} = L_1 y \tag{13a}$$

$$\frac{dy}{ds} = -\frac{x}{L_1} \tag{13b}$$

where $x = r/r_c$, $y = v_r/v_b$, $s = Kz$, and $L_1 = 1/Kr_c$. The subscript "1" on the quantity L_1 refers to the focusing cell. Eqs. (13a) and (13b) may be considered as the infinitessimal form of a mapping of the x-y plane into itself - they indicate how, for an infinitessimal increment in the parameter s, the points x and y transform. The geometric theory of ordinary differential equations[6] provides a method for building up the global transformation from the infinitessimal transformation. The global transformation is an operator known as the Lie transform which will be denoted here by Q. It is built by an exponentiation of the infinitessimal transformation. For a general differential system,

$$\frac{dx}{ds} = f(x,y) \tag{14a}$$

$$\frac{dy}{ds} = g(x,y) \tag{14b}$$

the operator Q is defined as

$$Q = \exp\left[s\left(f(x,y)\,\frac{\partial}{\partial x} - g(x,y)\,\frac{\partial}{\partial y} \right)\right] \tag{15}$$

This operator can be applied to any function of x and y to find how that function changes under the transformation defined by Eqs. (14a) and (14b). In particular, to obtain x(s), Q is applied to the function x, evaluated at s = 0. For Eqs. (13a) and (13b), the operator Q takes on the form

$$Q = \exp\left[s\left(L_1 y \frac{\partial}{\partial x} - \frac{1}{L_1} x \frac{\partial}{\partial y} \right)\right] \tag{16}$$

Using this to obtain x(s) gives

$$x(s) = x(0) + L_1 y(0) s - x(0)\frac{s^2}{2} - L_1 y(0)\frac{s^3}{6} + \ldots. \tag{17}$$

This can be recognized as the power series expansion of the exact solution of Eq. (13a):

$$x(s) = x(0)\cos(s) + L_1 y(0)\sin(s) \tag{18}$$

The Lie transform method provides two benefits. First, it allows a solution of the radial equation of motion to be found. Of course, in the more general case of a field that behaves as r^N, it may not be possible to find a closed form solution by recognizing the function represented by the the infinite series as could be done for the case N = 1, but at least every term of the series will be known so that as many terms as are considered to be necessary may be retained. Second, the Lie transform method works for any function of x and y. This is useful because rather than finding expressions for x(s) and y(s) individually, then inverting those expressions and inserting the results into Eq. (12), Eq. (12) can be transformed directly by application of the Lie transform.

For an azimuthal magnetic field of the form $B_\theta(r) = B_o(r/r_c)^N$, the radial equations of motion, after dropping the presently uninteresting $v_z(r)$ nonlinearity and dedimensionalizing as was done for Eqs. (11), are

$$\frac{dx}{ds} = L_1 y, \tag{19a}$$

$$\frac{dy}{ds} = -x^N/L_1. \tag{19b}$$

The operator Q for this differential system is

$$Q = \exp\left[s\left(L_1 y \frac{\partial}{\partial x} - \frac{1}{L_1} x^N \frac{\partial}{\partial y}\right)\right] \tag{20}$$

To test how well this method works, and in particular, to determine how many terms in the power series implied by the exponential function should be retained, Eq. (20) was used to compute the trajectory of an ion. Figure 3 shows the trajectory $r(z)$ for $0 \leq z \leq \pi/K$ (one half of a betatron wavelength) obtained from a numerical solution to Eqs. (19a) and (19b) for the case $N = 4$, $r(0) = r_c$, $v_r(0) = 0$. In Figure 4, the relative error between the numerical solution and the Lie transform solution is plotted for the range $0 \leq z \leq \pi/4K$ (one eighth of a betatron wavelength). The Lie transform solution used terms through the seventh order. As can been seen, the Lie transform series solution is in excellent agreement with the numerical solution, with the relative error not exceeding 0.01%. For propagation distances greater than an eighth of a betatron wavelength, the relative error grows much larger, as indicated in Figure 5 where the relative error between the numerical solution and the Lie transform solution is plotted for $0 \leq z \leq \pi/2K$ (one quarter of a

betatron wavelength). For greater propagation distances, the number of terms that must be retained in the Lie series to obtain the same degree of accuracy increases, but for the purposes of this calculation, where the propagation distance is limited to one eighth of a betatron wavelength, seven terms appear to be adequate.

For the purpose of predicting the spotsize, it is more convenient to apply the propagation operator Q directly to the function that defines the radial phase space boundary than to develop the solutions for the radius and the radial velocity individually, then combining those results to give the radial phase space boundary. This function, in terms of the dimensionless variables introduced above, is is

$$\rho^2(x,y) = x^2 + L_o y^2 - r_{ch}^2 = 0 \qquad (21)$$

Here, the subscript "0" on the quantity L_o refers to the dimensionless betatron wavelength in the transport channel. The ratio $R = (L_o/L_1)^2$ is equal to the ratio of the final focusing cell discharge current to the transport channel discharge current. The transformation of this boundary curve is illustrated in Figures 6a, 6b, and 6c for N = 2, 4, and 10, respectively. The deformation of the boundary curve is the sheared rotation anticipated previously.

In principle, the spotsize is predicted by applying the propagation operator Q to the function $\rho^2(x,y) - r_{ch}^2$, setting the result equal to zero, evaluating it at y = 0, then solving for x. Unfortunately, the resulting equation is a high-order polynomial in x. For example, for N = 2 and retaining terms through the fourth power in s gives the equation

$$0 = 1 - x^2 + x^3 s^2 - \left(x^4 s^2 - \frac{2}{3} x^5 s^4\right) R - \frac{5}{12} x^4 s^4 \qquad (22)$$

This, being a fifth order polynomial in x, cannot be solved by elementary means. While one could resort either to a numerical solution to Eq. (22) or to retaining fewer terms in the Lie transform power series, both of which are undesirable alternatives, neither are necessary because Eq. (22) can be solved for R, the ratio of currents, as a function of the spot size. The same situation holds true for any N and for any number of terms retained in the solution. Thus, while it is not generally possible to find an expression giving the spotsize as a function of the current ratio, it is possible in general to find an expression giving the current ratio as a function of the spotsize. The information content of the two is identical.

The current ratio necessary for producing a given spotsize has been obtained for N = 2, 3, ... by the means described above. The series expressions for $\rho^2(x,y)$ used for this purpose retained terms through the sixth order in s. The resulting expression is

$$R(x) = \left(\frac{1}{s^2 x^{2N}}\right) \left\{ \frac{1 - x^2 + s^2 x^{N+1} - \frac{s^4}{4!}[2(N+1)+4]x^{2N} + \frac{s^6}{6!}[8N(N+3)]x^{3N-1}}{1 - \frac{s^2}{3}Nx^{N-1} + \frac{s^4}{180}[N(2(3N-1) + 4(2N-1) + 3(N-1))]x^{2N-2}} \right\} . \qquad (23)$$

At the exit of the one-eighth betatron wavelength final focusing cell, $s = \pi/4$, and $x = x_{foc} = r_{foc}/r_c$. Note that for small spotsizes, the required current ratio is approximately $R(x_{foc}) \approx (4/\pi x_{foc}^N)^2$. Figure 7 displays the ratio of current as a function of spotsize for several different values of N and

different ranges of R. In this plot the current ratio for N = 1 as determined from Eq. (1) is shown for comparison. These results show, for example, that to produce a spotsize of $(1/2)r_c$, a current ratio of 7 is needed for N = 1, a ratio of 25.9 is needed for N = 2, and a ratio of 352.4 is needed for N = 4.

To find the focal length, the developments above are used to obtain an expression for the slope of the boundary curve at the spotsize radius. The boundary curve is propagated ballistically by replacing x with $\xi = x - y\Sigma$ and s with $\pi/4$, where $\Sigma = z/r_c$. The slope of the boundary curve is then found by differentiating the expression $\rho^2(\xi, y, \pi/4) - r_c^2 = 0$ with respect to x, and solving the resulting expression for $\partial y/\partial x$ yielding

$$\frac{\partial y}{\partial x} = \left[\frac{-\frac{\partial \rho}{\partial \xi}\frac{\partial \xi}{\partial x}}{\frac{\partial \rho}{\partial \xi}\frac{\partial \xi}{\partial y} + \frac{\partial \rho}{\partial y}} \right] \tag{24}$$

Using $\partial\xi/\partial x = 1$ and $\partial\xi/\partial y = -\Sigma$, and using the power series expansion of ρ^2 to evaluate the derivatives of ρ then gives the desired expression for the slope of the boundary curve. The focal length is given by the value of Σ at which $\partial y/\partial x \to -\infty$. This occurs when the denominator of the right-hand side of Eq. (24) vanishes. Thus, in general terms, the dimensionless focal length Σ_{foc} is

$$\Sigma_{foc} = \frac{\left(\frac{\partial \rho}{\partial y}\right)}{\left(\frac{\partial \rho}{\partial \xi}\right)} \tag{25}$$

Using the power series expression for ρ^2 and proceeding as indicated yields the expression

$$\Sigma_{foc} = \left(\frac{\pi}{4}\right)L_1\left\{2\left(Rx^{N-1} - 1\right) + \frac{1}{3}\left(\frac{\pi}{4}\right)^2\left[(N+3)x^{N-1} - 4NRx^{2N-2}\right] + \right. \tag{26}$$
$$\left. \frac{1}{30}\left(\frac{\pi}{4}\right)^4\left[RN\left(4(2N-1) + 3(N-1) + 2(3N-1)\right)x^{3N-2} - 2N(N+3)x^{2N-1}\right]\right\}$$

$$+ \left\{2 + \left(\frac{\pi}{4}\right)^2\left(2NRx^{2N-2} - (N+1)x^{N-1}\right) + \frac{1}{6}\left(\frac{\pi}{4}\right)^4\left(N(N+3)x^{2N-2} - 2N(3N-1)Rx^{3N-2}\right) + \right.$$
$$\left. \frac{1}{180}\left(\frac{\pi}{4}\right)^6\left[N(4N-2)\left(4(2N-1) + 3(N-1) + 2(3N-1)\right)Rx^{4N-4} - 2N(N+3)(3N-1)x^{3N-3}\right]\right\}$$

In this equation, the spotsize $x = x_{foc}$ and the current ratio R must be determined consistently using Eq. (23). The focal length is plotted in Figure 8 as a function of the spotsize for several different values of N. In this Figure, the focal length for the standard N = 1 cell was determined using Eq. (2). For values of the spotsize that are close to the channel radius, i.e. for x_{foc} near 1, the behavior of the focal length depends strongly on the number of terms retained in both the relation between x_{foc} and R and in the relation for Σ_{foc} indicating that higher order terms are needed for convergence. However, beam compression ratios near 1 are not of interest in this work. For the smaller values of x_{foc} which are of interest here, the number of terms retained in the Lie series is sufficient, allowing the focal lengths to be resolved with sufficient accuracy.

IV. Comparison of Theoretical Predictions with Numerical Simulations

The results of this analysis have been compared with numerical simulations of intense ion beam focusing. The simulation code used for this purpose was a simple ion trajectory solver. The trajectories of a large number (1000 - 5000) of ions are computed in a given magnetic field distribution. It is assumed that the ion beam is fully charge and current neutralized so that self fields can be neglected. It is also assumed that the magnetic field is static. Figure 9 shows the radial phase space distribution of 5100 ions at the entrance to the focusing cell. This distribution was obtained by phase averaging an initial phase space distribution in a 3 cm, 20 kA transport channel. The initial radial phase space distribution was a uniform distribution of ions in the rectangle $0 < r < 2.12$ cm and $0 < |v_r/v_b| < 0.053$. Figures 10a and 10b show the ion beam radial phase space distribution after passing through a focusing cell with $N = 2$ and $N = 4$, respectively. The ratio of the focusing cell discharge current to the transport channel discharge current was chosen to be 17, which for the $N = 1$ cell, gives a spotsize of $(1/3)r_c$. From Eq. (25), the spotsize for the $N = 2$ cell should be $0.552r_c$ and for the $N = 4$ cell, $0.721r_c$. Figures 11a and 11b show the radial phase space distributions for the $N = 2$ and $N = 4$ cells, respectively, after traveling through field free space to the theoretical focal plane. For the $N = 2$ cell, Eq. (30) predicts the focal length to be 7.50 cm and for the $N = 4$ cell, 5.51 cm. The comparison of the numerical simulation results with the theoretical predictions show that the theory accurately predicts the result of the numerical simulation; the spotsizes and the focal lengths from the code runs are very close to the theoretical predictions.

V. Conclusion

The spotsize and focal length of a one eighth betatron wavelength final focusing cell with the nonideal magnetic field distribution $B_\theta(r) = (2I_f/r_c c)\times(r/r_c)^N$ have been calculated. These results indicate that the ratio of final focusing cell discharge current to transport channel discharge current required for producing a given focused beam spotsize increases rapidly with increasing N. The focal length decreases with increasing N for any given spotsize. The very rapid increase in the current ratio required to produce a given spotsize with increasing N given by the approximate relation

$$\frac{I_f}{I_c} \sim \left(\frac{4}{\pi}\right)^2 \left(\frac{r_{foc}}{r_c}\right)^{-2N} \tag{27}$$

indicates that to be able to use the one-eighth betatron wavelength focusing technique without having to use mega-ampere level final focusing cell discharge currents requires that N be as close to 1 as possible. This, in turn, indicates the importance of understanding the development of the magnetic field in the final focusing cell.

Acknowledgements

This work was supported by the U.S. Department of Energy through Sandia National Laboratories. One of the authors (JW) was a National Research Council Associate at the Naval Research Laboratory during the time this work was being performed.

References

[1]C. L. Olson, in IEEE Conference Record-Abstracts, 1987 IEEE International Conference on Plasma Science (IEEE, New York, 1987), p. 27.

[2]P. F. Ottinger, Shyke A. Goldstein, and D. Mosher, NRL Memorandum Report 4948, Nov. 12, 1982.

[3]P. F. Ottinger, S. A. Goldstein, and D. Mosher, in IEEE Conference Record-Abstracts, 1981IEEE International Conference on Plasma Science (IEEE, New York, 1981, p. 98.

[4]J. Watrous, P. F. Ottinger, and D. Mosher, NRL Memorandum Report (in preparation).

[5]J. Neri, P. J. Goodrich, D. D. Hinshelwood, S. J. Stephanakis J. J. Watrous, and F. C. Young, Bull. Am. Phys. Soc. 32, 1878 (1987).

[6]G. W. Bluman and J. D. Cole, Similarity Methods for Differential Equations, New York: Springer-Verlag, 1974.

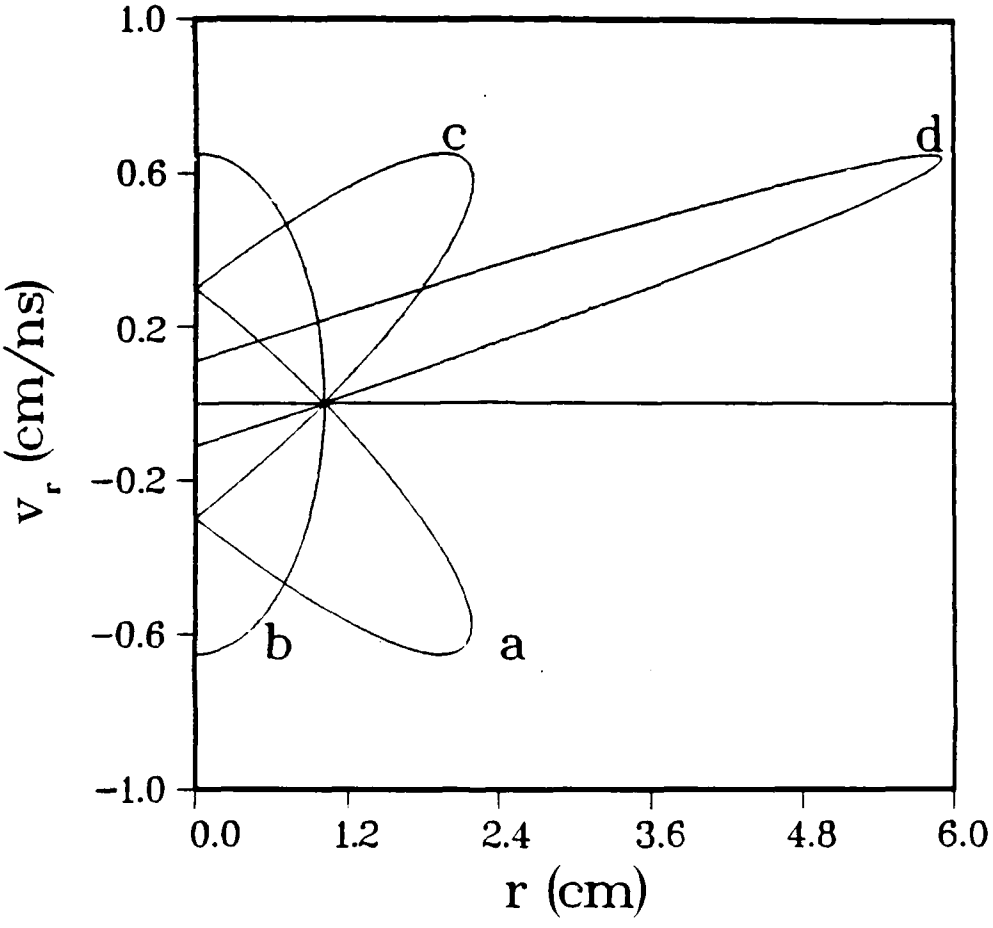

Figure 1: Illustration of the general theoretical method for determining the spotsize of the focused ion beam. Curve (a) represents the boundary curve at the final focusing cell exit. As the beam propagates ballistically, the intersection of the boundary curve with the line $v_r = 0$ does not change. Curves (b), (c), and (d) represent the boundary curve after ballistic propagation through distances of z_{foc}, $2z_{foc}$, and $4z_{foc}$, respectively.

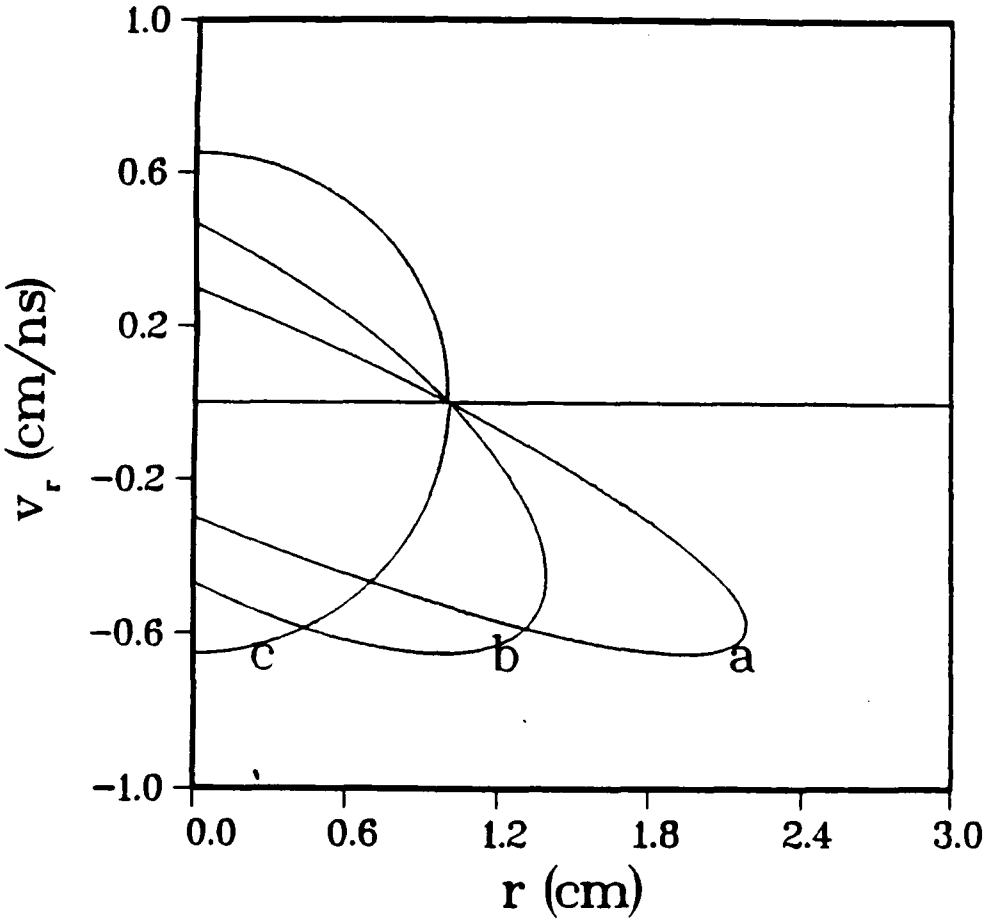

Figure 2: Illustration of the general theoretical method for determining the focal length of the final focusing cell. As the ion beam leaves the final focusing cell and propagates ballistically, the tangent to the boundary curve at the intersection with the v_r axis approaches $-\infty$. Curve (a) represents the boundary curve at the final focusing cell exit. Curves (b) and (c) represent the boundary curve after ballistic propagation through distances of $(1/2)z_{foc}$ and z_{foc}, respectively.

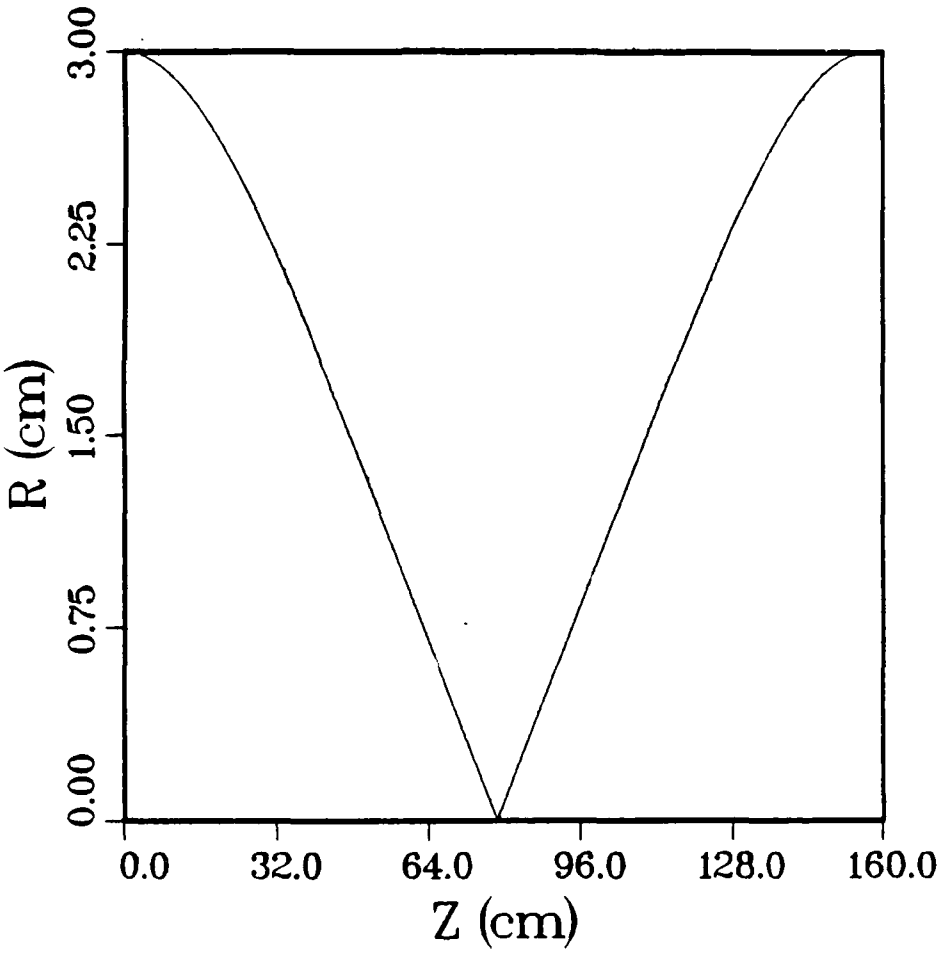

Figure 3: Trajectory of a beam ion calculated numerically using Eqs. (19a) and (19b). The magnetic field exponent N was 4, and the initial conditions were $r(0) = r_c$, $v_r(0) = 0$. One half of a betatron oscillation is shown. The discharge current was 20 kA, the channel radius was 3 cm, and the beam ions were 30 MeV Li^{+3}_{7}.

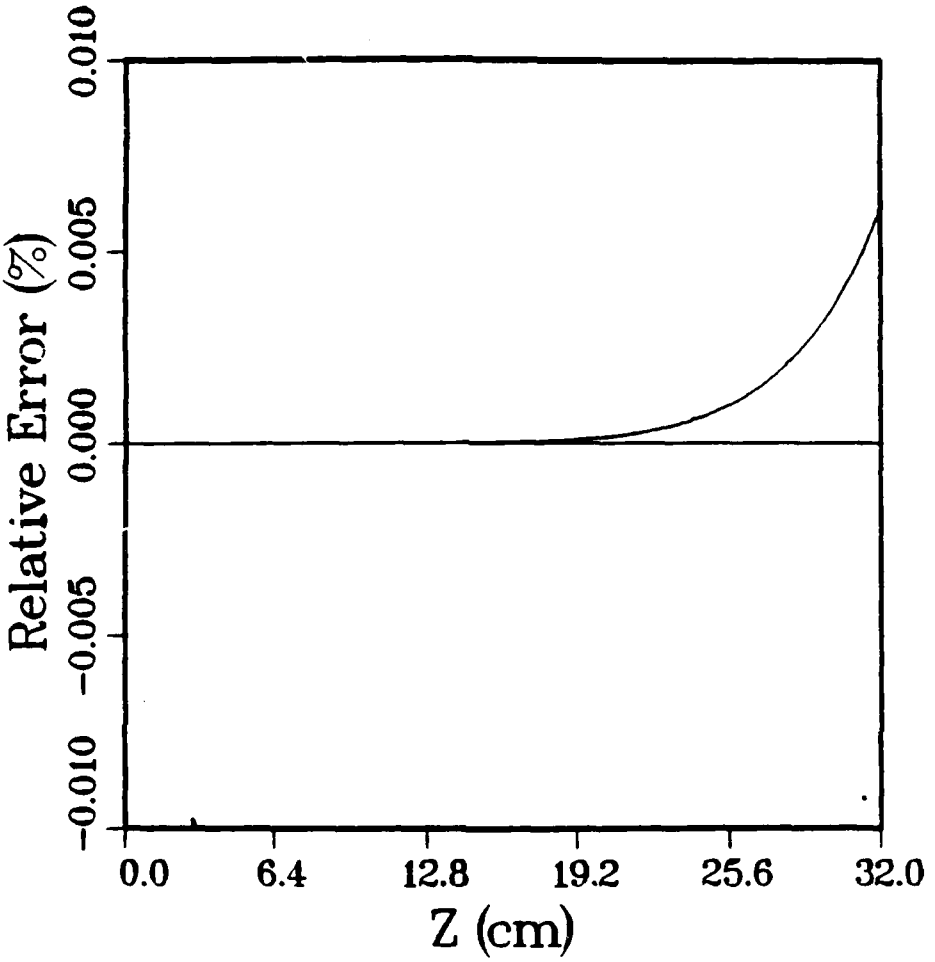

Figure 4: The relative error between the numerical solution and the Lie transform solution over one eighth of a betatron wavelength. The Lie transform solution used terms through the seventh order.

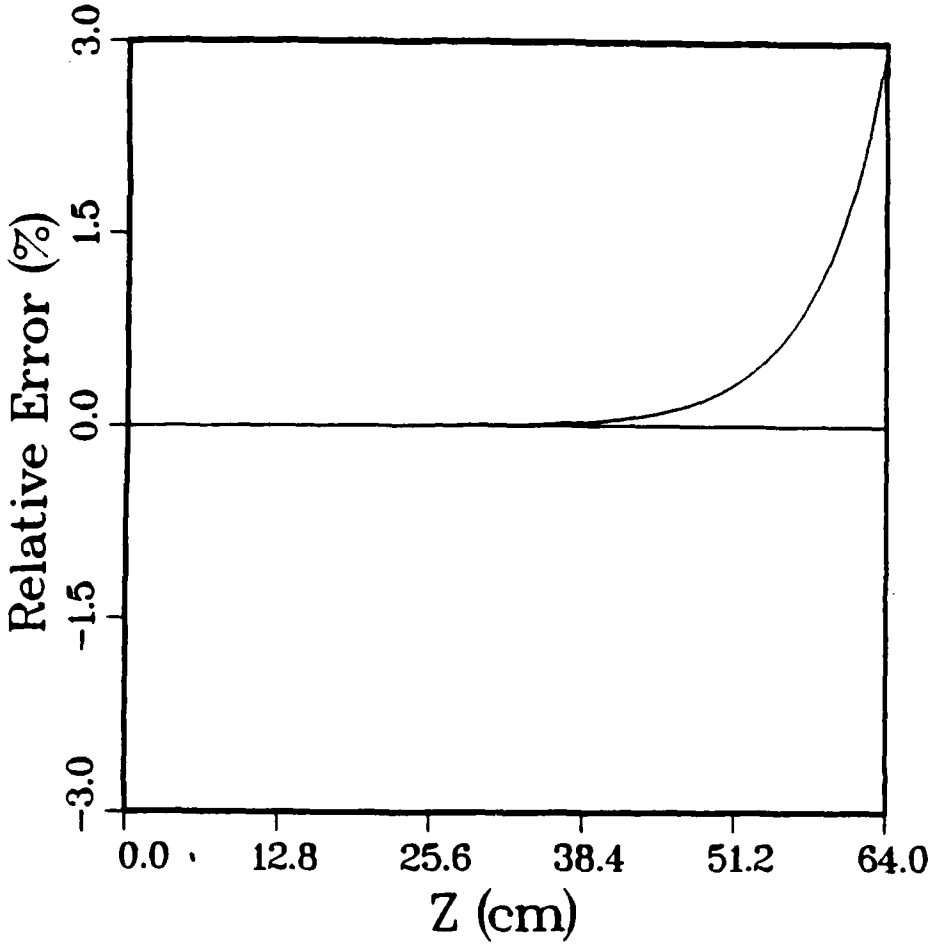

Figure 5: The relative error between the numerical solution and the Lie transform solution over one quarter of a betatron wavelength. The Lie transform solution used terms through the seventh order.

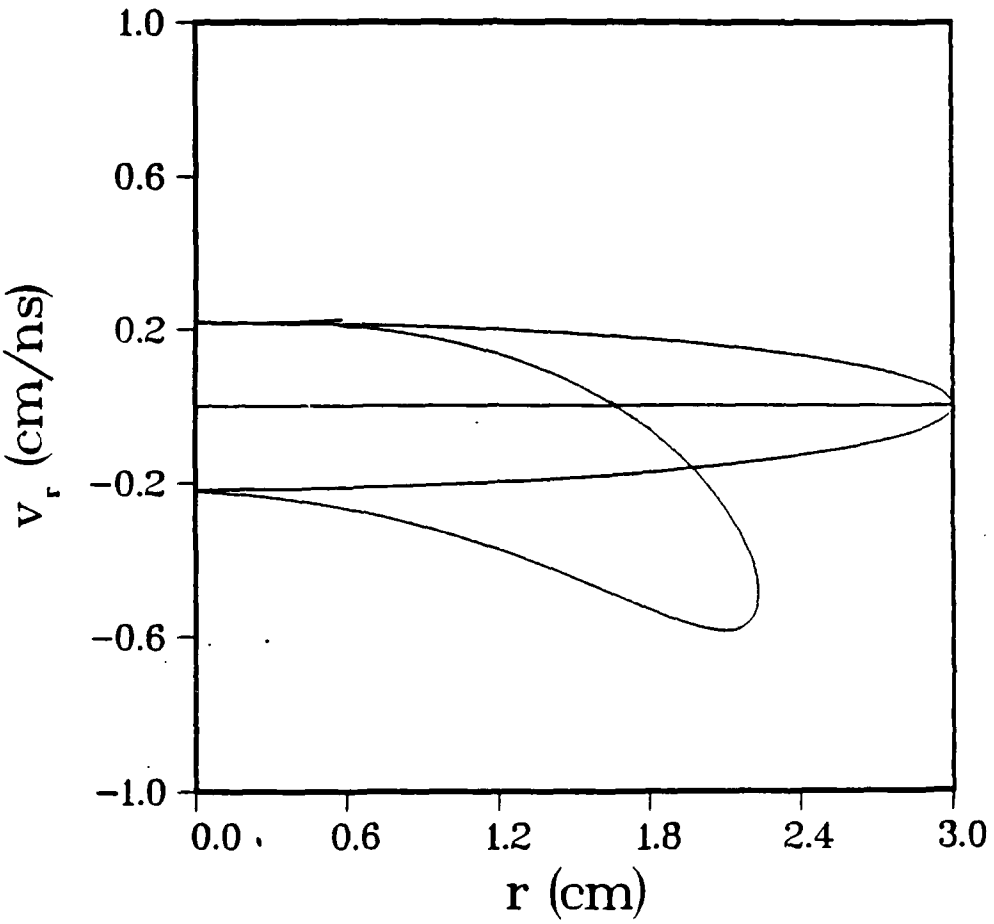

Figure 6a: Transformation of the boundary curve for N = 2.

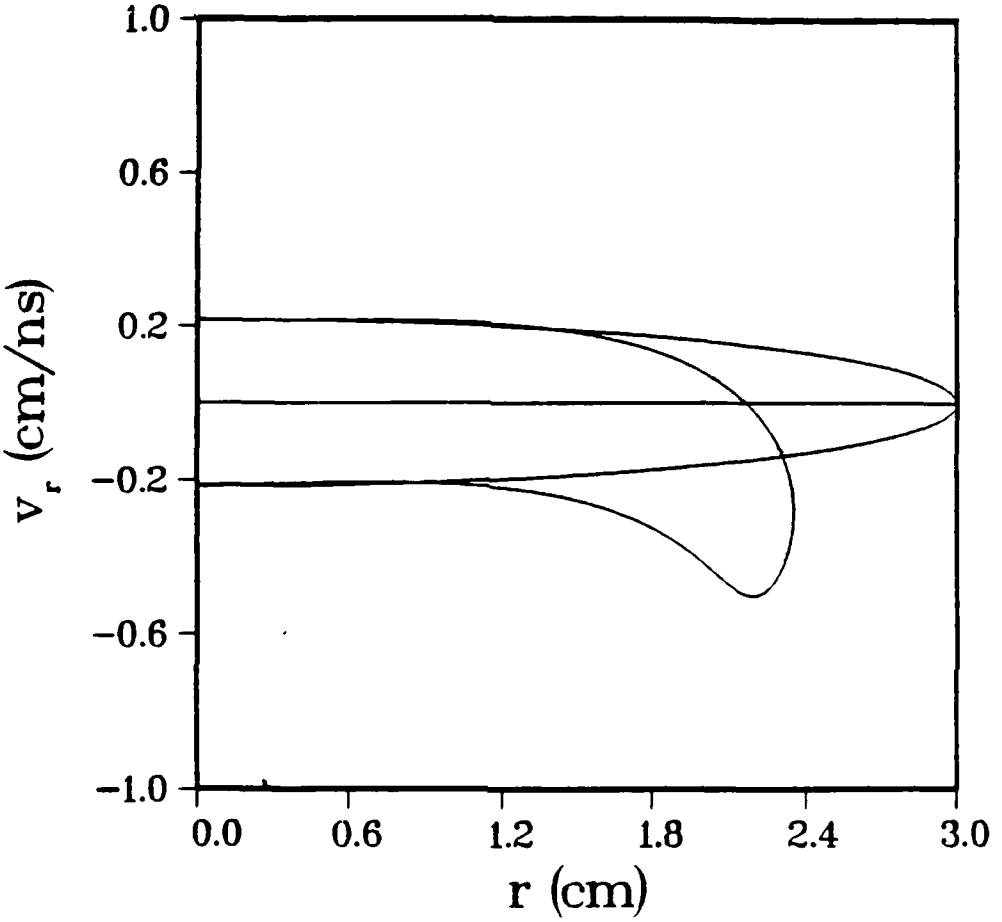

Figure 6b: Transformation of the boundary curve for N = 4.

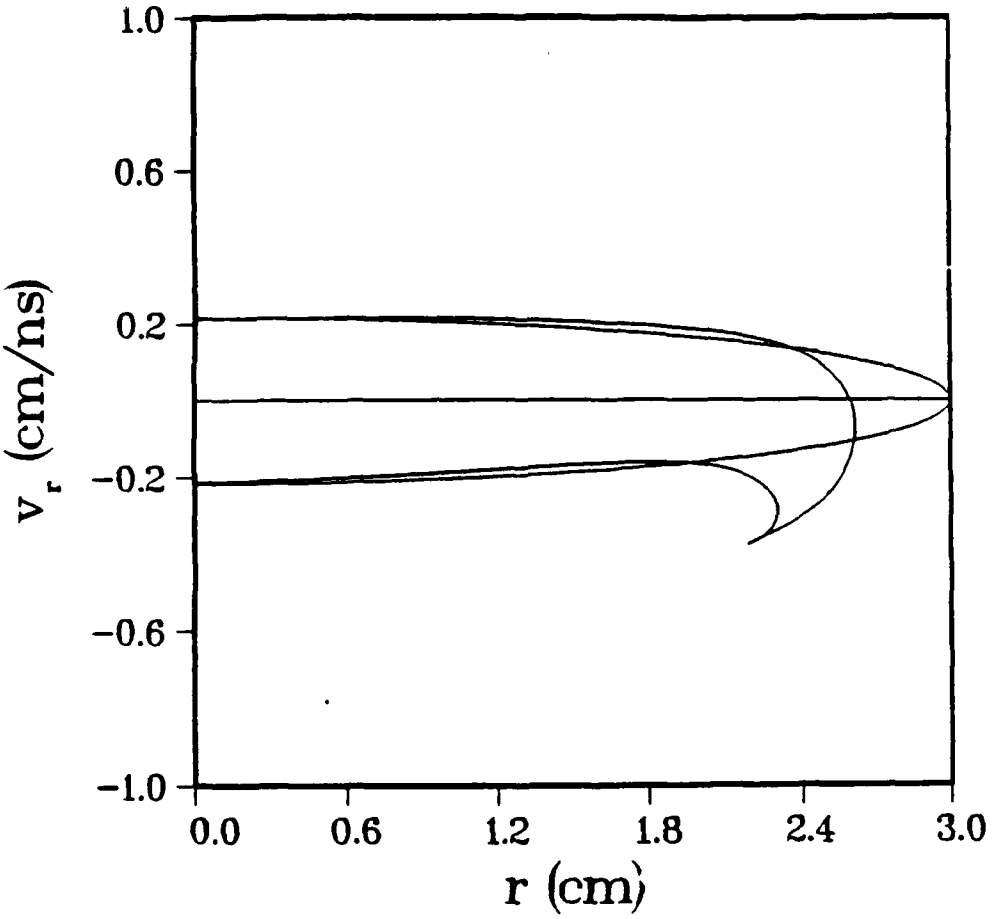

Figure 6c: Transformation of the boundary curve for N = 10.

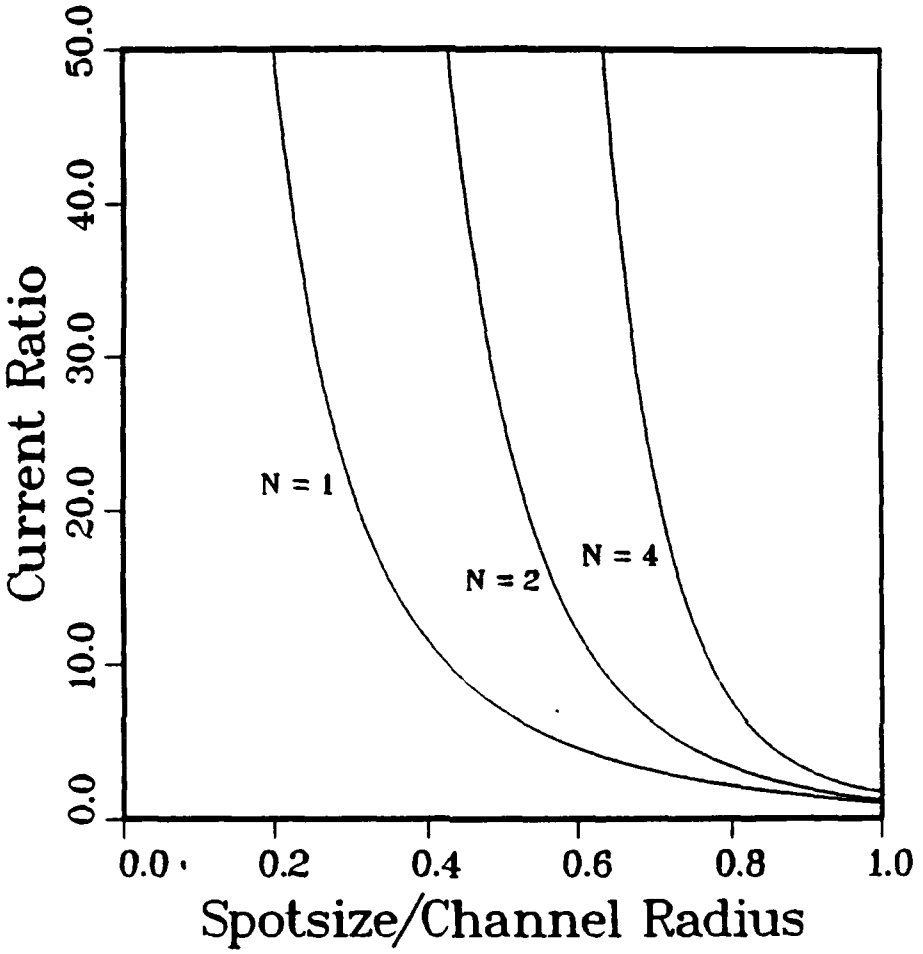

Figure 7: Ratio of discharge currents required to produce a given spotsize for N = 1, N = 2, and N = 4.

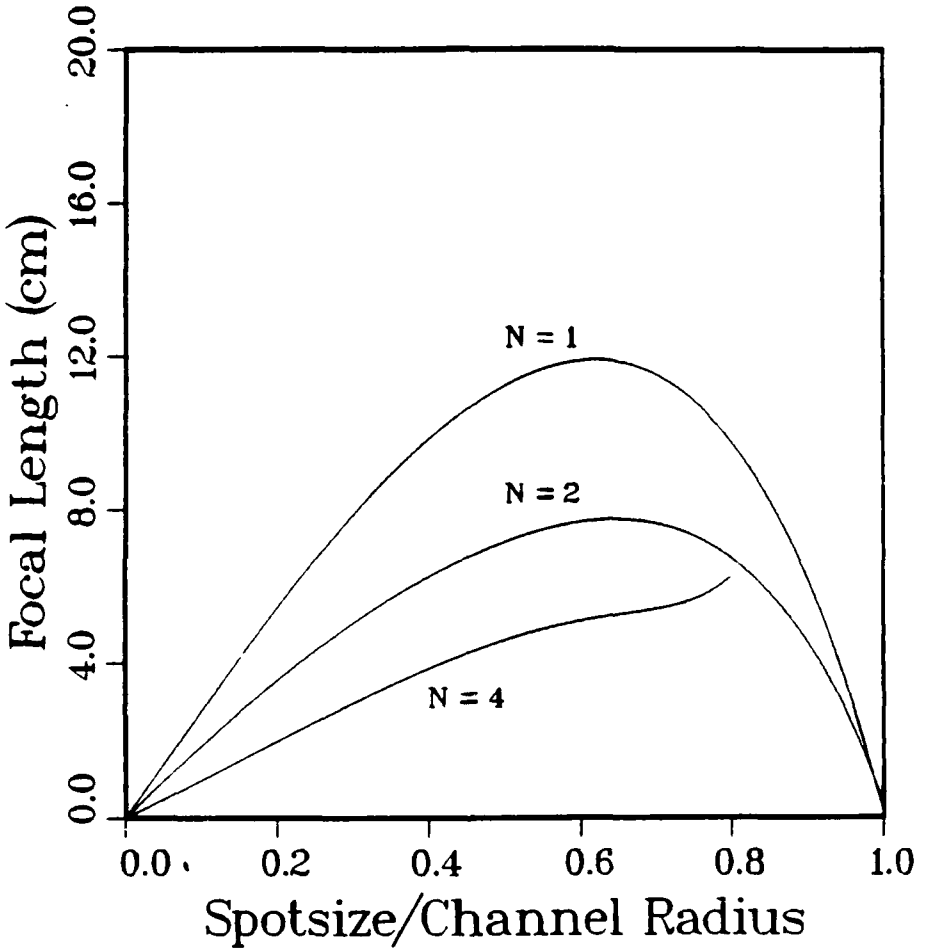

Figure 8: Focal length for final focusing cells with N = 1, N = 2, and N = 4.

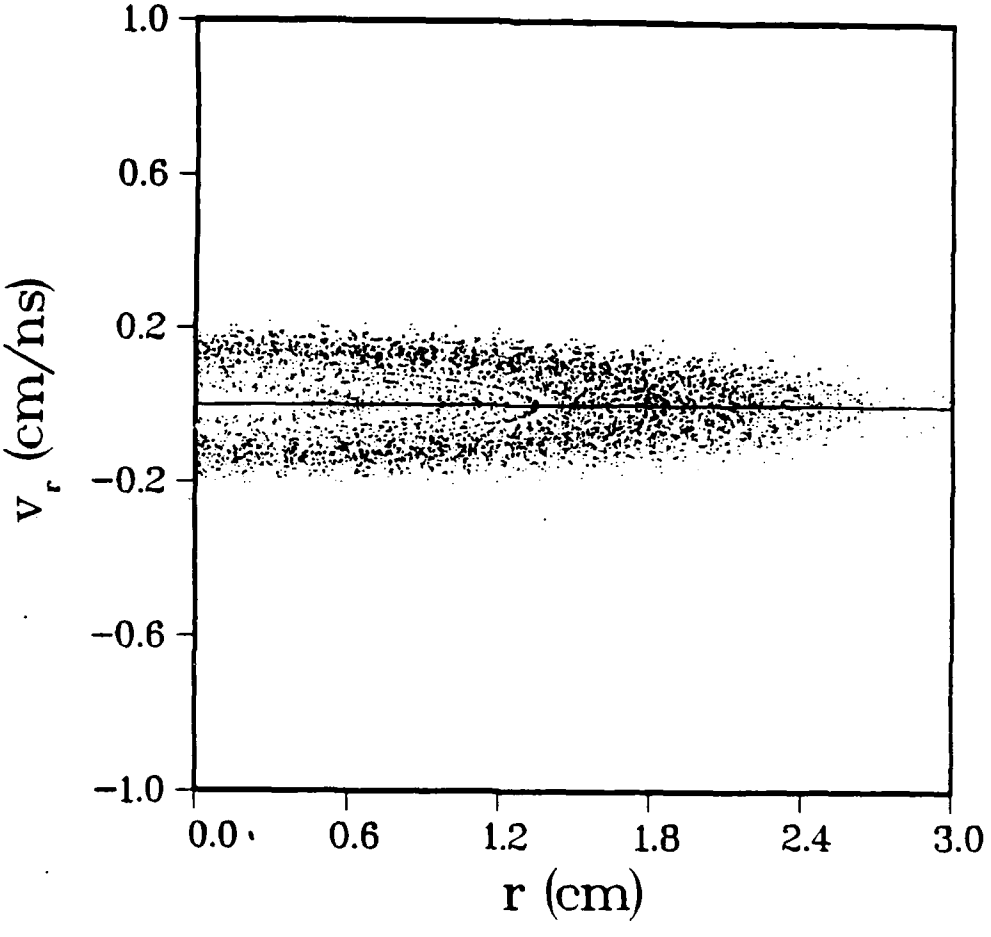

Figure 9: Radial phase space distribution at the entrance to the final focusing cell used for the numerical simulation.

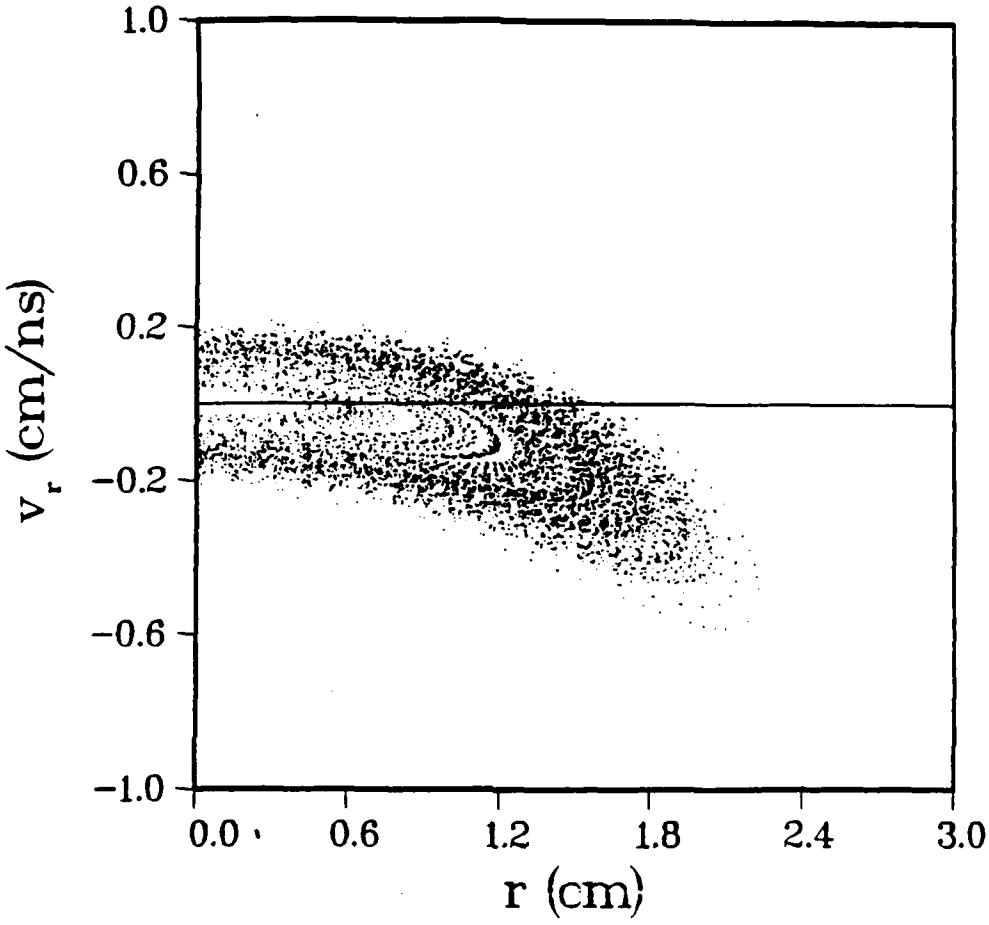

Figure 10a: Radial phase space distribution at the final focusing cell exit obtained from the numerical simulation of an N = 2 cell. Theory predicts that the intersection between the boundary curve and the v_r axis should occur at $0.552r_c$.

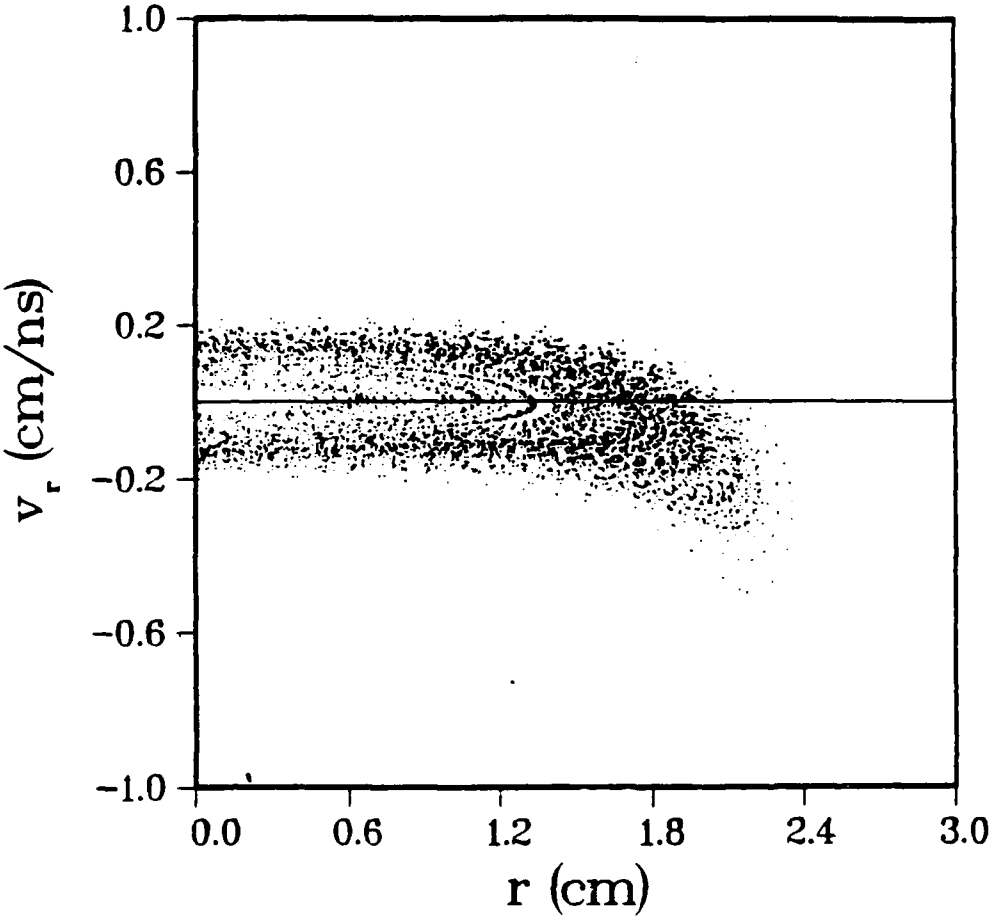

Figure 10b: Radial phase space distribution at the final focusing cell exit obtained from the numerical simulation of an N = 4 cell. Theory predicts that the intersection between the boundary curve and the v_r axis should occur at $0.721r_c$.

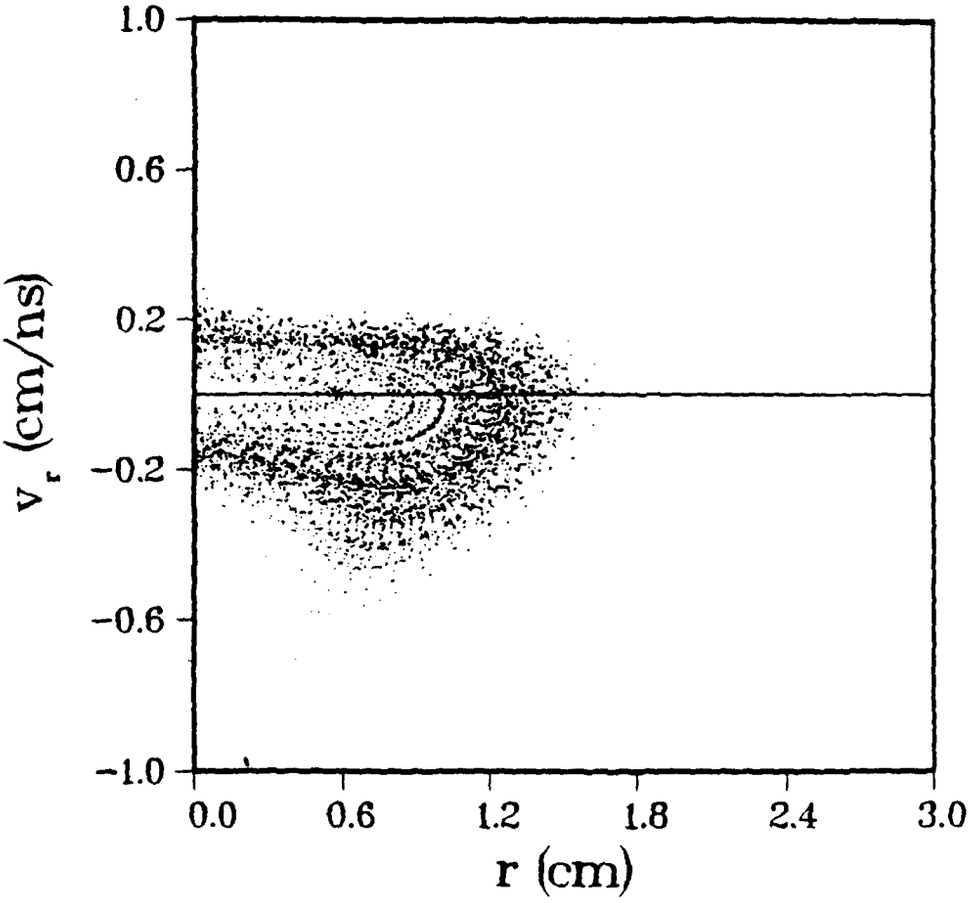

Figure 11a: Radial phase space distribution after 7.50 cm of ballistic propagation. The theory predicts that at this location, all ions should be located within the spotsize radius.

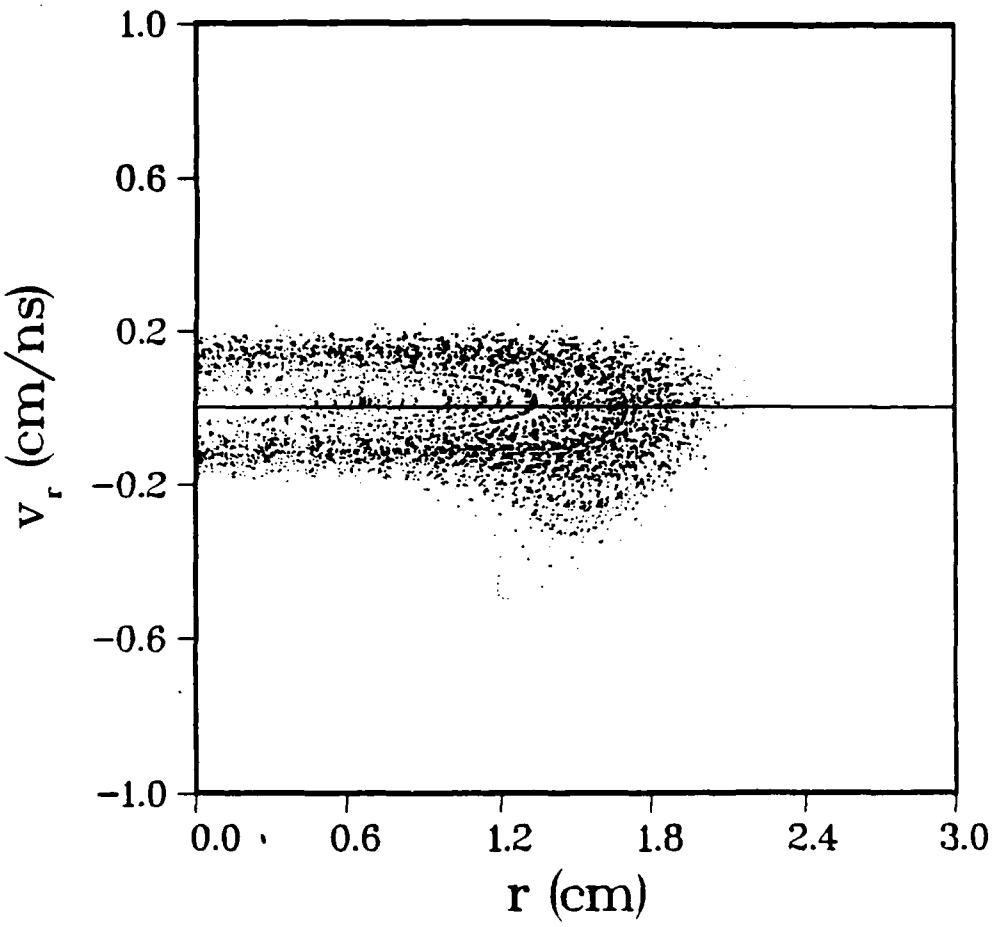

Figure 11b: Radial phase space distribution after 5.51 cm of ballistic propagation. The theory predicts that at this location, all ions should be located within the spotsize radius.

DISTRIBUTION FOR DOE SPONSORED WORK
15 March 1988

U.S. Department of Energy
Office of Inertial Fusion
Washington, DC 20545
Attn: S.L. Kahalas — 1 copy
R.L. Schriever — 1 copy

U.S. Department of Energy
Office of Classification
Washington, DC 20545
Attn: Robert T. Duff — 1 copy

U.S. Department of Energy
Nevada Operations Office
P.O. Box 14100
Las Vegas, NV 89114 — 2 copies

U.S. Department of Energy
P.O. Box 62
Oak Ridge, TN 37830 — 1 copy

Cornell University
Ithaca, NY 14850
Attn: D.A. Hammer — 1 copy
R.N. Sudan — 1 copy

Defense
Technical Information Center Station
Duke Street
Alexandria, VA 22314
Attn: T.C. — 2 copies

JAYCOR, Inc.
1608 Spring Hill Rd.
Vienna, VA 22180-2270
Attn: B.V. Weber — 1 copy
D.D. Hinshelwood — 1 copy

KMS Fusion, Inc.
3941 Research Park Drive
P.O. Box 1567
Ann Arbor, MI 48106
Attn: A.A. Glass — 1 copy

Lawrence Berkley Laboratory
Berkley, CA 94720
Attn: D. Keefe — 1 copy

Director of Research
U.S. Naval Academy
Annapolis, MD 21402 — 2 copies

Code 1220 — 1 copy

Records — 1 copy

Code 2634 Cindy Sims — 1 copy

Lawrence Livermore National Laboratory
P.O. Box 808
Livermore, CA 94550
Attn: R. Batzel/J. Kahn, L-1 — 1 copy
J. Emmett, 1-488 — 1 copy
W. Krupke, L-488 — 1 copy
E. Storm, L-481 — 1 copy
J. Lindl, L-477 — 1 copy

Los Alamos Scientific Laboratory
P.O. Box 1663
Los Alamos, NM 87545
Attn: S.D. Rockwood,
ICF Prog. Mgr.
DAD/IF/M/S 527 — 1 copy

Naval Research Laboratory
4555 Overlook Ave., S.W.
Washington, D.C. 20375-5000
Attn: Code/Name

2628/TID Dist	22 copies
1000/T. Coffey	1 copy
4000/W. Ellis	1 copy
4040/J. Boris	1 copy
4700/S.L. Ossakow	26 copies
4701/I. Vitkovitsky	1 copy
4710/C. Kapetanakos	1 copy
4720/J. Davis	1 copy
4730/S. Bodner	1 copy
4740/W. Manheimer	1 copy
4750/R. Meger	1 copy
4760/B. Robson	1 copy
4770/G. Cooperstein	10 copies
4770.1/F. Young	1 copy
4770.1/D. Mosher	1 copy
4770.2/R. Co ..nisso	1 copy
4771/P. Ottinger	1 copy
4771/J. Neri	1 copy
4771/J. Grossmann	1 copy
4773/S. Stephanakis	1 copy
4790/D. Colombant	1 copy
4790/I. Haber	1 copy
4790/M. Lampe	1 copy
4600/D. Nagel	1 copy

Sandia National Laboratories
P.O. Box 5800
Albuquerque, NM 87185
Attn: J.P. VanDevende-/1200 — 1 copy
D.L. Cook/1250 — 5 copies
T. Martin/1250 — 1 copy

University of Rochester
250 East River Road
Rochester, NY 14623
Attn: J. Eastman — 1 copy